ORIGINAL ARTICLE

lajss.org Latin American Journal of Solids and Structures www.lajss.org

Free vibration and buckling analysis of bio-inspired helicoid laminated composite plates resting on Pasternak foundation using the first-order meshfree

Thanh Son Doan[a], Trung Thanh Tran[b], Pham Hong Thao[c]*, Huy Gia Luong[d], Ngoc-Tu Do[e]

[a]Faculty of Automotive Engineering, School of Technology, Van Lang University, Ho Chi Minh City, Vietnam. Email: son.dt@vlu.edu.vn
[b]Faculty of Mechanical Engineering, Le Quy Don Technical University, Hanoi, Vietnam. Email: tranthanh0212@gmail.com
[c]Faculty of Engineering and Technology, Nguyen Tat Thanh University, Ho Chi Minh City, Vietnam. Email: phthao@ntt.edu.vn
[d]TechnoStar Vietnam, TechnoStar Co. Ltd, Ho Chi Minh City, Vietnam. Email: giahuy@e-technostar.com
[e]Faculty of Industrial Systems, School of Mechanical and Automotive Engineering, Hanoi University of Industry, Hanoi, Vietnam. Email: tudn@haui.edu.vn

*Corresponding author

https://doi.org/10.1590/1679-7825/e8346

Abstract
This article investigates the buckling and free vibration behavior of bio-inspired helicoid laminated composite (BiHLC) plates resting on a Pasternak foundation (PF) using the meshfree moving Kriging (MK) method for the first time. In this study, the MK method leverages Reddy's first-order shear deformation theory (FSDT) for analysis of the mechanical behavior of plates. The PF is characterized by two stiffness parameters: spring stiffness k_1 and shear stiffness k_2. A key advantage of the MK interpolation is its Kronecker's delta property, enabling direct enforcement of boundary conditions (BC). Unlike original MK method, this approach does not require pre-defining the correlation parameter, which can influence approximation accuracy. The governing equations are derived using Hamilton's principle. A thorough analysis is conducted to understand how the helicoidal layup scheme, geometrical parameters, BC, and the foundation's stiffness parameters influence the critical buckling loads and natural frequencies of BiHLC plates.

Keywords
Bio-inspired helicoidal; Laminated plate; Pasternak foundation; Moving Kriging; FSDT.

Received August 21, 2024. In revised form October 30, 2024. Accepted November 15, 2024. Available online November 20, 2024.
https://doi.org/10.1590/1679-7825/e8346

Graphical Abstract

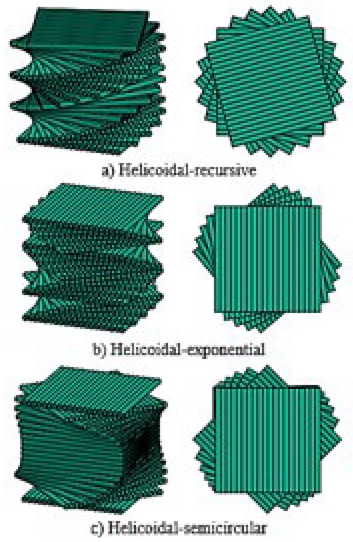

The helicoidal schemes

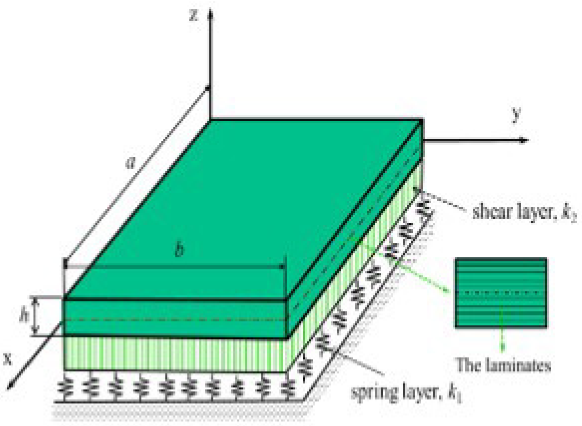

The model of BiHLC plate resting on PF.

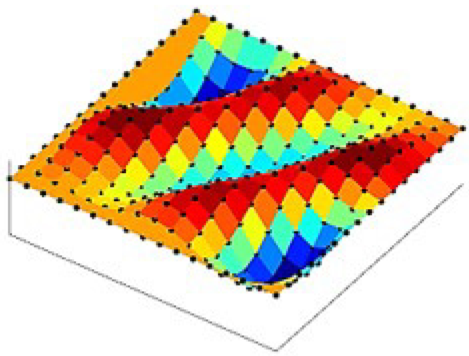

Mode 6: $N_6^n = 146.6865$

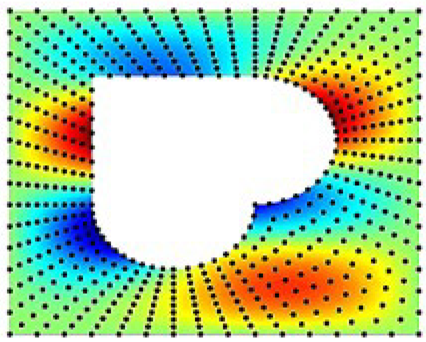

Mode 6: $\omega_6^n = 59.6440$

NOMENCLATURE

BiHLC: Bio-inspired helicoid laminated composite
PF: Pasternak foundation
MK: Moving Kriging
FSDT: First-order shear deformation theory
BC: Boundary conditions
ESL: Equivalent single layer
CPT: Classical plate theory
EF: Elastic foundations
FGP: Functionally graded plate
RPIM: Radial point interpolation method
HR: Helicoidal recursive
HE: Helicoidal exponential
HS: Helicoidal semicircular
NOL: Number of lamina

1 INTRODUCTION

The field of bio-inspired structures is experiencing a surge in research due to its potential to revolutionize engineering design. This approach leverages the ingenious strategies evolved in nature to tackle complex engineering challenges, particularly in the area of energy absorption. As highlighted by San Ha and Lu (2020), publications are rapidly increasing, showcasing advancements in biomimetic structures for this purpose. Building on this, Greco et al. (2023) explores the design of optimized configurations using additive manufacturing techniques, further boosting energy absorption capabilities. Beyond energy absorption, bio-inspired structures offer a wider range of benefits. Works like Kiakojouri, De Biagi and Abbracciavento (2023) delve into biomimetic solutions for structural robustness, categorized as compartmentalization and complexity. Honeycomb structures, inspired by nature, are a prime example. Studies such as Sherman, Zhang and Xu (2021); Liu et al. (2022b, 2023) highlight their advantages: superior strength-to-weight ratios and enhanced energy absorption, making them ideal for aerospace, automotive, and protective gear applications. Similarly, bio-inspired laminates offer improved damage tolerance, enhanced mechanical properties, and increased durability, as emphasized in Wenting et al. (2021); Lu et al. (2023). By mimicking natural designs, researchers can create high-performance materials that are not only strong and lightweight but also adaptable to diverse conditions. Some studies such as Do et al. (2023); Do and Pham (2023) investigate vibration behavior of BiHLC plate under different loads and computational models. Greenfeld and Wagner (2023) takes inspiration from scorpion exoskeletons, investigating how variations in stiffness and thickness within laminate layers can deflect cracks. Inspired by natural laminated composites with helical arrangements, researchers like Han et al. (2020); Liu et al. (2020); Körbelin et al. (2021); Wang et al. (2021) have studied the impact of foreign objects on these structures. Paruthi et al. (2023) further explores this concept by comparing the free vibration and buckling behavior of double-helicoidal and cross-helicoidal bio-inspired laminated composite plates under thermal conditions. Finally, Meo et al. (2021) delves into the design and manufacturing of Functionally Graded Pitch laminated composites, exploiting the toughness of variable-angle helical structures to improve impact resistance.

Several review articles explore the analysis of laminated composite plates and shells using various plate theories. Odeh et al. (2024) categorizes models by treating the laminate as a single layer, examining how established theories differ. Reddy (2003) focus on common Equivalent Single Layer (ESL) theories like Classical Plate Theory (CPT) and FSDT, highlighting their use in design, analysis, and optimization of composite structures. Khandan et al. (2012) provide a comprehensive review, classifying theories into single-layer, layerwise (including zig-zag and discrete), and mixed (hybrid) approaches. Building on existing work, Gao et al. (2022) propose a novel bending model for composite laminated shells based on a refined zig-zag theory. Additionally, various methods for analyzing the mechanical behavior of composite plates are explored in the literature Zheng et al. (2021); Bakoura et al. (2022); Cho and Ahn (2022); Zhou, Cui and Wen (2022); Adim and Hassaine Daouadji (2023).

The mechanical behavior of structures on elastic foundations (EF) has been a well-studied topic. The foundation models are commonly used in studies such as WF (one-parameter model) by Katsikadelis and Armenakas (1984); Yokoyama (1988), PF is a two-parameter model by Pasternak (1954), and KF (three-parameter model) by Kerr (1964). Then, several key works have explored various aspects: Guellil et al. (2021) investigated the impact of porosity distributions on the bending response of functionally graded plates using the Navier solution. Hadji et al. (2023) analyzed the combined influence of porosity and EF on the bending behavior of sandwich structures. Zaitoun et al. (2023) examined the vibration of FG sandwich plates on viscoelastic foundations using a high-order shear deformation theory. Additionally, studies by Merazka et al. (2021); Mudhaffar et al. (2021) explored the hygrothermo-mechanical response of functionally graded (FG) plates on EFs. Recent works by Hebali et al. (2022); Liu et al. (2022a); Tahir et al. (2022) have also provided insights into the influence of EF on the mechanical response of plates.

Meshfree methods, when combined with enriched terms Fleming et al. (1997); Pant, Singh and Mishra (2010); Nguyen et al. (2014); Nguyen, Bui and Truong (2017); Bui et al. (2018); Nguyen et al. (2020), offer an increasingly attractive approach for tackling fracture problems. Unlike traditional methods reliant on meshes, meshfree approaches provide significant flexibility. This flexibility arises from discretizing the problem domain using only nodes, eliminating the need for elements, mesh generation, or sub-triangulation. Additionally, meshfree methods often leverage higher-order shape functions, potentially leading to improved accuracy. However, within the meshfree class, only the radial point interpolation method (RPIM), e.g. Wang and Liu (2002) and the MK method, e.g. Gu (2003); Bui, Nguyen and Nguyen-Dang (2009) possess the crucial Kronecker delta property. This property enables the direct enforcement of BC, a critical aspect of many simulations. Interestingly, a strong connection between RPIM and MK has been established in Dai et al. (2003). This finding has spurred the application of MK to plate analysis. For instance, Thai et al. (2018) presents a MK meshfree method based on naturally stabilized nodal integration. They employ this method for bending, free vibration, and buckling analyses of isotropic and functionally graded sandwich plates within the framework of higher-order shear deformation theories. Besides, Vu-Tan and Phan-Van (2018) introduced a modified MK interpolation-based meshfree method with refined sinusoidal shear deformation theory to analyze FG plates. Do and Pham (2023) studied the dynamic response of BiHLC plates resting on EF by using IGA. Furthermore, Le and Van Do (2024) combines the MK meshfree method with a simple Kirchhoff theory to analyze the natural frequency and thermal buckling deformations of advanced material plates. In another study, Thai et al. (2016) presents a global MK interpolation-based meshfree method for static, free vibration, and buckling analyses of isotropic plates.

It can be seen that the studies on BiHLC structural analysis are mainly static problems, natural vibration problems and dynamic response problems using standard FEM or IGA. At the same time, meshfree is also an advanced numerical method with great potential in modeling and analyzing complex structures supported by EF. Besides, our evaluation of the results demonstrates that the combined MK and FSDT method offers a highly suitable approach for structural analysis. This method achieves good accuracy with a straightforward model, making it computationally efficient. The novelty of this work is for the first time the MK model without the need for user-defined parameters based on Reddy's FSDT for buckling and free vibration analysis of BiHLC plates on PFs. Unlike the original MK method, this approach does not require pre-defining the correlation parameter, which can influence approximation accuracy. The governing equations are derived using Hamilton's principle. Furthermore, we present detailed new numerical results that explore the influence of factors such as helicoidal layup scheme, geometrical parameters, BC, and foundation stiffness on the buckling and free vibration behavior of BiHLC plates. We believe this study provides a valuable foundation for scientists and engineers working on the research and design of military equipment, including tanks, armored vehicles, missiles, submarines, and combat aircraft.

2 BIO-INSPIRED HELICOID LAMINATED COMPOSITE PLATE RESTING ON PASTERNAK FOUNDATION

This study investigates three distinct helicoidal designs: helicoidal recursive (HR), helicoidal exponential (HE), and helicoidal semicircular (HS). Their configurations are presented in Figure 1 and summarized in Table 1 for easy reference.

Table 1 The configuration of the helicoidal layup scheme via number of lamina.

.	**Helicoidal recursive (HR): $\alpha_1/\alpha_2/\alpha_3/\ldots\alpha_n = \alpha_{n-1} + \beta(n-1)$**		
	Type 1 ($\beta = 1$)	Type 2 ($\beta = 2$)	Type 3 ($\beta = 3$)
12	[0/1/3/6/10/15]$_s$	[0/2/6/12/20/30]$_s$	[0/3/9/18/30/45]$_s$
16	[0/1/3/6/10/15/21/28]$_s$	[0/2/6/12/20/30/42/56]$_s$	[0/3/9/18/30/45/63/84]$_s$
20	[0/1/3/6/10/15/21/28/36/45]$_s$	[0/2/6/12/20/30/42/56/72/90]$_s$	[0/3/9/18/30/45/63/84/108/135]$_s$
24	[0/1/3/6/10/15/21/28/36/45/55/66]$_s$	[0/2/6/12/20/30/42/56/72/90/110/132]$_s$	[0/3/9/18/30/45/63/84/108/135/165/198]$_s$
28	[0/1/3/6/10/15/21/28/36/45/55/66/78/91]$_s$	[0/2/6/12/20/30/42/56/72/90/110/132/156/182]$_s$	[0/3/9/18/30/45/63/84/108/135/165/198/234/273]$_s$
	Helicoidal exponential (HE): $\alpha_1/\alpha_2/\alpha_3/\ldots\alpha_n = \gamma^n$		
	Type 1 ($\gamma = 2$)	Type 2 ($\gamma = 2.5$)	Type 3 ($\gamma = 3$)
12	[2/4/8]$_{2s}$	[2.5/6.3/15.6]$_{2s}$	[3/9/27]$_{2s}$
16	[2/4/8/16]$_{2s}$	[2.5/6.3/15.6/39]$_{2s}$	[3/9/27/81]$_{2s}$
20	[2/4/8/16/32]$_{2s}$	[2.5/6.3/15.6/39/97.7]$_{2s}$	[3/9/27/81/243]$_{2s}$
24	[2/4/8/16/32/64]$_{2s}$	[2.5/6.3/15.6/39/97.7/244.1]$_{2s}$	[3/9/27/81/243/729]$_{2s}$
28	[2/4/8/16/32/64/128]$_{2s}$	[2.5/6.3/15.6/39/97.7/244.1/610.4]$_{2s}$	[3/9/27/81/243/729/2187]$_{2s}$
	Helicoidal semicircular (HS): $\alpha_1/\alpha_2/\alpha_3/\ldots\alpha_n = \sqrt{\mu^2 - (\psi(n-1) - \mu)^2}$		
	Type 1 ($\mu = 45$)	Type 2 ($\mu = 90$)	Type 3 ($\mu = 180$)
12	[0/27/36/41.3/44.1/45]$_s$	[0/54/72/82.5/88.2/90]$_s$	[0/108/144/165/176.4/180]$_s$
	$\psi = 9$	$\psi = 18$	$\psi = 36$
16	[0/23.3/31.6/37/40.8/43.2/44.6/45]$_s$	[0/46.6/63.3/74.2/81.6/86.5/89.2/90]$_s$	[0/93.2/126.6/148.3/163.2/173/178.4/180]$_s$
	$\psi = 6.5$	$\psi = 13$	$\psi = 26$
20	[0/20.6/28.3/33.5/37.4/40.3/42.4/43.9/44.7/45]$_s$	[0/41.2/56.5/67.1/74.8/80.6/84.9/87.7/89.4/90]$_s$	[0/82.5/113.1/134/149.7/161.2/169.7/175.5/ 178.9/180]$_s$
	$\psi = 5$	$\psi = 10$	$\psi = 20$
24	[0/18.6/25.6/30.6/34.4/37.4/39.8/41.6/ 43.1/44.1/44.7/45]$_s$	[0/37.1/51.2/61.2/68.8/74.8/79.6/83.3/86.2/ 88.2/89.4/90]$_s$	[0/74.2/102.4/122.4/137.6/149.7/159.2/166.6/ 172.3/176.3/178.9/180]$_s$
	$\psi = 4$	$\psi = 8$	$\psi = 16$
28	[0/17.4/24.1/28.9/32.6/35.6/38.1/40.1/41.7/ 42.9/43.9/44.5/44.8/45]$_s$	[0/34.8/48.2/57.8/65.2/71.2/76.1/80.1/83.3/ 85.9/87.7/89/89.8/90]$_s$	[0/69.6/96.4/115.6/130.5/142.5/152.3/160.2/ 166.7/171.7/175.5/178.1/179.6/180]$_s$
	$\psi = 3.5$	$\psi = 7$	$\psi = 14$

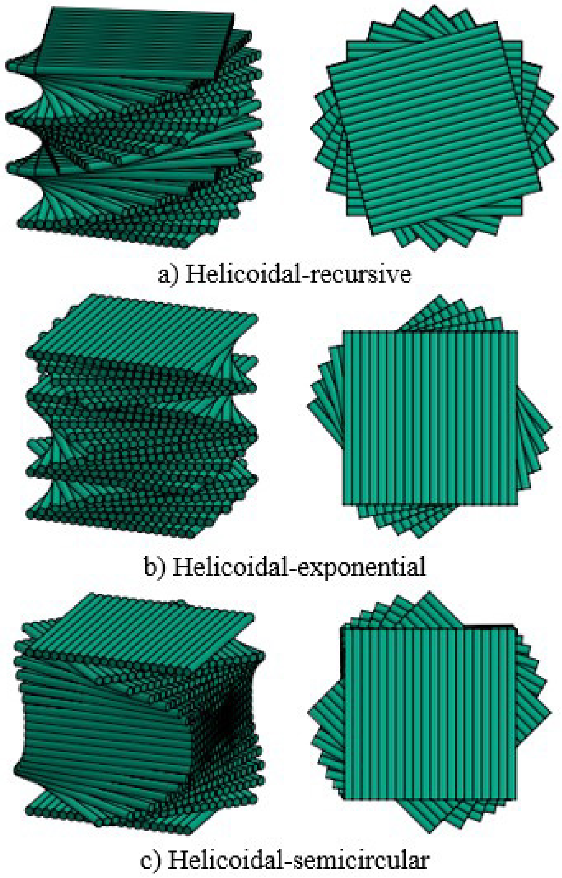

Figure 1. The helicoidal schemes are based on the study of Jiang et al. (2019).

The BiHLC plate with geometrical parameters as show in Figure 2. The PF model is an extension of the Winkler foundation model that takes into account the shear interaction between the spring elements. The PF model is described by the following differential equation as Keshtegar et al. (2020).

$$\mathcal{R} = k_1 w_0 - k_2 \left(\frac{\partial^2 w_0}{\partial x^2} + \frac{\partial^2 w_0}{\partial y^2}\right) \tag{1}$$

where k_1 is the spring stiffness or Winkler parameter, k_2 is the shear stiffness or shear foundation parameter.

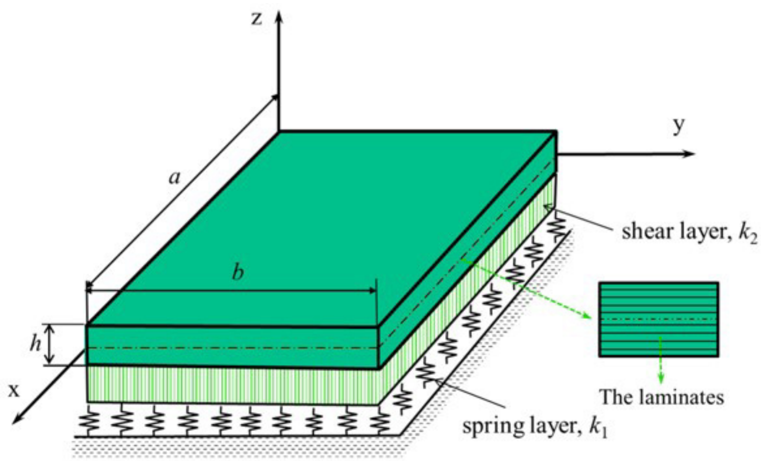

Figure 2. The model of BiHLC plate resting on PF.

3 THEORETICAL FORMULATION

3.1 Meshfree moving Kriging interpolation

In recent years, the MK method has gained significant traction due to its appealing properties. This meshfree approach utilizes Gaussian semivariogram model to construct shape functions, offering advantages in terms of stability and eliminating the use of shape parameter (Bui et al., 2018). Consider a scalar field $\mathbf{u}(\mathbf{x})$ defined within a support domain denoted by $\Omega_x \subseteq \Omega$. This field is represented by a set of scattered nodes $\mathbf{x}_i$ $(i = 1, \ldots, n)$. The MK method allows to approximate the value of $\mathbf{u}(\mathbf{x})$ at any point of interest $\mathbf{x}$ using the following formula:

$$\boldsymbol{u}^h(\boldsymbol{x}) = [\boldsymbol{p}^T(\boldsymbol{x})\boldsymbol{M} + \boldsymbol{R}^T(\boldsymbol{x})\boldsymbol{N}]\boldsymbol{u}(\boldsymbol{x}) \tag{2}$$

or

$$\boldsymbol{u}^h(\boldsymbol{x}) = \sum_{i=1}^{n} \boldsymbol{\varphi}_i(\boldsymbol{x})\boldsymbol{u}_i \tag{3}$$

with $\mathbf{p}(\mathbf{x})$ and $\mathbf{R}(\mathbf{x})$ are the vectors of polynomial and radial basis function, respectively.

$$\boldsymbol{p}(\boldsymbol{x}) = [\boldsymbol{p}_1(\boldsymbol{x}) \quad \ldots \quad \boldsymbol{p}_2(\boldsymbol{x}) \quad \boldsymbol{p}_m(\boldsymbol{x})]^T \tag{4}$$

$$\boldsymbol{R}(\boldsymbol{x}) = [\boldsymbol{R}(\boldsymbol{x}_1, \boldsymbol{x}) \quad \ldots \quad \boldsymbol{R}(\boldsymbol{x}_2, \boldsymbol{x}) \quad \boldsymbol{R}(\boldsymbol{x}_n, \boldsymbol{x})]^T \tag{5}$$

The shape function in the node i-th can be written as:

$$\boldsymbol{\varphi}_i(\boldsymbol{x}) = \sum_{j=1}^{m} \boldsymbol{p}_j(\boldsymbol{x})\boldsymbol{M}_{ji} + \sum_{k=1}^{n} \boldsymbol{r}_k(\boldsymbol{x})\boldsymbol{N}_{ki} \tag{6}$$

The matrices $\mathbf{M}$ and $\mathbf{N}$ are determined via:

$$\boldsymbol{M} = (\boldsymbol{P}^T\boldsymbol{R}^{-1}\boldsymbol{P})^{-1}\boldsymbol{P}^T\boldsymbol{R}^{-1} \tag{7}$$

$$\boldsymbol{N} = \boldsymbol{R}^{-1}(\boldsymbol{I}^0 - \boldsymbol{P}\boldsymbol{M}) \tag{8}$$

in which $\mathbf{I}^0$ denotes the unit matrix, the matrix $\mathbf{P}$ is the moment matrix of polynomial basis functions and $\mathbf{R}$ is moment matrix of correlation functions with the explicit form as:

$$\boldsymbol{P} = \begin{bmatrix} \boldsymbol{p}_1(\boldsymbol{x}_1) & \boldsymbol{p}_2(\boldsymbol{x}_1) & \cdots & \boldsymbol{p}_m(\boldsymbol{x}_1) \\ \boldsymbol{p}_1(\boldsymbol{x}_2) & \boldsymbol{p}_2(\boldsymbol{x}_2) & \cdots & \boldsymbol{p}_m(\boldsymbol{x}_2) \\ \vdots & \vdots & \ddots & \vdots \\ \boldsymbol{p}_1(\boldsymbol{x}_n) & \boldsymbol{p}_2(\boldsymbol{x}_n) & \cdots & \boldsymbol{p}_m(\boldsymbol{x}_n) \end{bmatrix}_{(\boldsymbol{n}\times\boldsymbol{m})} \tag{9}$$

$$\boldsymbol{R} = \begin{bmatrix} \mathbf{1} & \boldsymbol{R}(\boldsymbol{x}_1, \boldsymbol{x}_2) & \cdots & \boldsymbol{R}(\boldsymbol{x}_1, \boldsymbol{x}_n) \\ \boldsymbol{R}(\boldsymbol{x}_2, \boldsymbol{x}_1) & \mathbf{1} & \cdots & \boldsymbol{R}(\boldsymbol{x}_2, \boldsymbol{x}_n) \\ \vdots & \vdots & \ddots & \vdots \\ \boldsymbol{R}(\boldsymbol{x}_n, \boldsymbol{x}_1) & \boldsymbol{R}(\boldsymbol{x}_n, \boldsymbol{x}_2) & \cdots & \mathbf{1} \end{bmatrix}_{(\boldsymbol{n}\times\boldsymbol{n})} \tag{10}$$

In this study, the quadratic polynomial $\mathbf{p}(\mathbf{x}) = [1 \quad x \quad y \quad x^2 \quad y^2 \quad xy]$ with $m = 6$ is chosen for calculation. Several correlation functions are applicable to $\mathbf{R}$, as explored in Bui et al. (2018). This work departs from the conventional MK method Gu (2003) by employing a Gaussian correlation function without the need for user-defined parameters. The chosen correlation function is

$$\boldsymbol{R}(\boldsymbol{x}_i, \boldsymbol{x}_j) = \boldsymbol{e}^{\left(-\frac{1}{2l_c^2}\right)r_{ij}^2} \tag{11}$$

where r_{ij} is the distance between the point of interest $\mathbf{x}$ and node at $\mathbf{x_i}$, l_c captures the characteristic length scale within the support domain and is computed as the average distance between nodes. The second derivatives of the shape functions are also presented due to the requirements of the calculations related to the PF

$$\boldsymbol{\varphi}_{i,l}(\boldsymbol{x}) = \sum_{j=1}^{m} \boldsymbol{p}_{j,l}(\boldsymbol{x})\boldsymbol{M}_{ji} + \sum_{k=1}^{n} \boldsymbol{r}_{k,l}(\boldsymbol{x})\boldsymbol{N}_{ki} \tag{12}$$

$$\boldsymbol{\varphi}_{i,ll}(\boldsymbol{x}) = \sum_{j=1}^{m} \boldsymbol{p}_{j,ll}(\boldsymbol{x})\boldsymbol{M}_{ji} + \sum_{k=1}^{n} \boldsymbol{r}_{k,ll}(\boldsymbol{x})\boldsymbol{N}_{ki} \tag{13}$$

where l represents either the x or y coordinate. A comma following l indicates a partial differentiation with respect to the corresponding spatial coordinate.

MK shape functions offer two key properties: partition of unity and Kronecker-delta function. These functions achieve interpolation at a specific point by considering a surrounding area called the support domain, which includes multiple field nodes. This domain, typically a circle in 2D problems and a sphere in 3D, is centered at a specific point of interest and defined by a radius. It essentially identifies the set of scattered nodes that contribute to the approximation of the solution at that point. The size of this influence domain is determined using a specific expression, detailed as Bui and Nguyen (2013)

$$d_m = \alpha d_c \tag{14}$$

here, d_c represents the characteristic length relative to the nodal spacing, and α acts as a scaling factor.

3.2 The first-order laminated plate theory

Following Reddy's FSDT Reddy (2003), the displacement field can be explained as

$$\begin{aligned} u(x,y,z) &= u_0(x,y) + z\phi_x(x,y) \\ v(x,y,z) &= v_0(x,y) + z\phi_y(x,y) \\ w(x,y,z) &= w_0(x,y) \end{aligned} \tag{15}$$

where u_0, v_0, and w_0 represent the in-plane (x, y) and out-of-plane (z) displacements of a midplane point. ϕ_x and ϕ_y denote rotations of the y-axis and x-axis, respectively. Strain-displacement relations are derived based on Von Kármán assumptions neglecting the normal transverse strain ε_z and infinitely small quantities are obtained as Reddy (2003)

$$\begin{Bmatrix} \boldsymbol{\varepsilon_{xx}} \\ \boldsymbol{\varepsilon_{yy}} \\ \boldsymbol{\gamma_{xy}} \end{Bmatrix} = \begin{Bmatrix} \frac{\partial u_0}{\partial x} \\ \frac{\partial v_0}{\partial y} \\ \frac{\partial u_0}{\partial y} + \frac{\partial v_0}{\partial x} \end{Bmatrix} + \boldsymbol{z} \begin{Bmatrix} \frac{\partial \phi_x}{\partial x} \\ \frac{\partial \phi_y}{\partial y} \\ \frac{\partial \phi_x}{\partial y} + \frac{\partial \phi_y}{\partial x} \end{Bmatrix} = \boldsymbol{\varepsilon_m} + \boldsymbol{z\varepsilon_b} \tag{16}$$

$$\begin{Bmatrix} \boldsymbol{\gamma_{xz}} \\ \boldsymbol{\gamma_{yz}} \end{Bmatrix} = \begin{Bmatrix} \frac{\partial w_0}{\partial x} + \boldsymbol{\phi_x} \\ \frac{\partial w_0}{\partial y} + \boldsymbol{\phi_y} \end{Bmatrix} = \boldsymbol{\gamma_s} \tag{17}$$

Considering a rectangular plate with total thickness h composed of various orthotropic layers. Because the plate is made of multiple layers of orthotropic material, typically with different properties, the constitutive equations of each layer need to be transformed from the material coordinate system to the global coordinates system. The stress-strain relations for the k-th layer in laminate coordinates are given by

$$\boldsymbol{\sigma_m} = \begin{Bmatrix} \boldsymbol{\sigma_{xx}} \\ \boldsymbol{\sigma_{yy}} \\ \boldsymbol{\tau_{xy}} \end{Bmatrix} = \begin{bmatrix} \overline{\boldsymbol{Q}}_{11} & \overline{\boldsymbol{Q}}_{12} & \overline{\boldsymbol{Q}}_{16} \\ \overline{\boldsymbol{Q}}_{21} & \overline{\boldsymbol{Q}}_{22} & \overline{\boldsymbol{Q}}_{26} \\ \overline{\boldsymbol{Q}}_{61} & \overline{\boldsymbol{Q}}_{62} & \overline{\boldsymbol{Q}}_{66} \end{bmatrix}^{(\boldsymbol{k})} \begin{Bmatrix} \boldsymbol{\varepsilon_x} \\ \boldsymbol{\varepsilon_y} \\ \boldsymbol{\gamma_{xy}} \end{Bmatrix} = \overline{\boldsymbol{Q}}_{\boldsymbol{m}}(\boldsymbol{\varepsilon_m} + \boldsymbol{z\varepsilon_b}) \tag{18}$$

$$\boldsymbol{\tau_s} = \begin{Bmatrix} \boldsymbol{\tau_{xz}} \\ \boldsymbol{\tau_{yz}} \end{Bmatrix} = \begin{bmatrix} \overline{\boldsymbol{Q}}_{44} & \overline{\boldsymbol{Q}}_{45} \\ \overline{\boldsymbol{Q}}_{54} & \overline{\boldsymbol{Q}}_{55} \end{bmatrix}^{(\boldsymbol{k})} \begin{Bmatrix} \boldsymbol{\gamma_{xz}} \\ \boldsymbol{\gamma_{yz}} \end{Bmatrix} = \overline{\boldsymbol{Q}}_{\boldsymbol{s}}\boldsymbol{\gamma_s} \tag{19}$$

where $\overline{Q}_{ij}$ are the transformed material constants which are given as Thai and Choi (2013)

$$
\begin{aligned}
\overline{Q}_{11} &= Q_{11}cos^4\theta + 2(Q_{12} + 2Q_{66})cos^2\theta sin^2\theta + Q_{22}sin^4\theta \\
\overline{Q}_{12} &= (Q_{11} + Q_{22} - 4Q_{66})cos^2\theta sin^2\theta + Q_{12}(cos^4\theta + sin^4\theta) \\
\overline{Q}_{16} &= (Q_{11} - Q_{12} - 2Q_{66})cos^3\theta sin\theta + (Q_{12} - Q_{22} + 2Q_{66})cos\theta sin^3\theta \\
\overline{Q}_{22} &= Q_{11}sin^4\theta + Q_{22}cos^4\theta + 2(Q_{12} + 2Q_{66})cos^2\theta sin^2\theta \\
\overline{Q}_{26} &= (Q_{12} - Q_{22} + 2Q_{66})cos^3\theta sin\theta + (Q_{11} - Q_{12} - 2Q_{66})cos\theta sin^3\theta \\
\overline{Q}_{66} &= (Q_{11} + Q_{22} - 2Q_{12} - 2Q_{66})cos^2\theta sin^2\theta + Q_{66}(cos^4\theta + sin^4\theta) \\
\overline{Q}_{44} &= Q_{44}cos^2\theta + Q_{55}sin^2\theta \\
\overline{Q}_{45} &= (Q_{55} - Q_{44})cos\theta sin\theta \\
\overline{Q}_{55} &= Q_{55}cos^2\theta + Q_{44}sin^2\theta
\end{aligned} \tag{20}
$$

in which θ is the angle between the x-axis of the global coordinate and the x_1-axis of the material coordinate, Q_{ij} are the reduced stiffness constants in the material coordinate given as

$$
\begin{aligned}
&Q_{11} = \frac{E_{11}}{1 - \nu_{12}\nu_{21}}, Q_{12} = \frac{\nu_{12}E_{22}}{1 - \nu_{12}\nu_{21}}, Q_{22} = \frac{E_{22}}{1 - \nu_{12}\nu_{21}}, \\
&Q_{66} = G_{12}, Q_{44} = G_{23}, Q_{55} = G_{13}
\end{aligned} \tag{21}
$$

3.3 Governing equation

The governing equations for this theory are derived by applying Hamilton's Principle Reddy (2003)

$$0 = \int_0^T \left(\delta U + \delta U_f + \delta V - \delta K\right) dt \tag{22}$$

where δU, δU_f, δV and δK represent the variations of strain energy, foundation strain energy, potential energy, and kinetic energy, respectively. The variation of strain energy is then expressed as

$$
\begin{aligned}
\boldsymbol{\delta U} &= \frac{1}{2}\int_V (\boldsymbol{\sigma_m^T \varepsilon_m} + \boldsymbol{z\sigma_m^T \varepsilon_b} + \boldsymbol{\tau_s^T \gamma_s})\boldsymbol{dV} \\
&= \frac{1}{2}\int_{\boldsymbol{\Omega}} (\boldsymbol{\varepsilon_m}^T \boldsymbol{A\varepsilon_m} + \boldsymbol{\varepsilon_b}^T \boldsymbol{B\varepsilon_m} + \boldsymbol{\varepsilon_m}^T \boldsymbol{B\varepsilon_b} + \boldsymbol{\varepsilon_m}^T \boldsymbol{D\varepsilon_m} + \boldsymbol{\gamma_s}^T \boldsymbol{A_s\gamma_s})\boldsymbol{d\Omega}
\end{aligned} \tag{23}
$$

in which the stiffness coefficients matrix $\mathbf{A}$, $\mathbf{B}$, $\mathbf{D}$ and $\mathbf{A}_s$ are defined by

$$(\boldsymbol{A}, \boldsymbol{B}, \boldsymbol{D}) = \int_{-h/2}^{h/2} (1, z, z^2)\overline{\boldsymbol{Q}}_{\boldsymbol{m}}\, dz \tag{24}$$

$$\boldsymbol{A_s} = \frac{5}{6}\int_{-h/2}^{h/2} \overline{\boldsymbol{Q}}_{\boldsymbol{s}}\, \boldsymbol{dz} \tag{25}$$

The variation of foundation strain energy is given by the following equation

$$\delta U_f = \frac{1}{2}\int_\Omega \delta w_0{}^T \left[k_1 w_0 - k_2\left(\frac{\partial^2 w_0}{\partial x^2} + \frac{\partial^2 w_0}{\partial y^2}\right)\right] d\Omega \tag{26}$$

The variation of potential energy is

$$\boldsymbol{\delta V} = \frac{1}{2}\int_\Omega \left\{ \boldsymbol{h\nabla^T \delta w_0 \widehat{\sigma}_0 \nabla w_0} + \boldsymbol{h}[\boldsymbol{\nabla^T \delta u_0} \quad \boldsymbol{\nabla^T \delta v_0}] \begin{bmatrix} \boldsymbol{\widehat{\sigma}_0} & \boldsymbol{0} \\ \boldsymbol{0} & \boldsymbol{\widehat{\sigma}_0} \end{bmatrix} \begin{bmatrix} \boldsymbol{\nabla u_0} \\ \boldsymbol{\nabla v_0} \end{bmatrix} + \frac{\boldsymbol{h^3}}{\boldsymbol{12}} [\boldsymbol{\nabla^T \delta \phi_x} \quad \boldsymbol{\nabla^T \delta \phi_y}] \begin{bmatrix} \boldsymbol{\widehat{\sigma}_0} & \boldsymbol{0} \\ \boldsymbol{0} & \boldsymbol{\widehat{\sigma}_0} \end{bmatrix} \begin{bmatrix} \boldsymbol{\nabla \phi_x} \\ \boldsymbol{\nabla \phi_y} \end{bmatrix} \right\} \boldsymbol{d\Omega} \tag{27}$$

where $\nabla^T = [\partial/\partial x \quad \partial/\partial y]^T$ and $\widehat{\boldsymbol{\sigma}}_0$ is the initial stress matrix as

$$\boldsymbol{\widehat{\sigma}_0} = \begin{bmatrix} \boldsymbol{\sigma_x^0} & \boldsymbol{\tau_{xy}^0} \\ \boldsymbol{\tau_{xy}^0} & \boldsymbol{\sigma_y^0} \end{bmatrix} = \begin{bmatrix} \boldsymbol{N_x^0/h} & \boldsymbol{N_{xy}^0/h} \\ \boldsymbol{N_{xy}^0/h} & \boldsymbol{N_y^0/h} \end{bmatrix} \tag{28}$$

In this study, uniaxial compression is considered the sole initial condition for the buckling analysis. Therefore, the in-plane forces acting in the vertical and horizontal directions, denoted by N_x^0, N_y^0, and N_{xy}^0, are simplified as follows:

$$N_x^0 = N^0;\ N_y^0 = N_{xy}^0 = 0 \tag{29}$$

The variations of kinetic energy can be written as

$$\boldsymbol{\delta K} = \frac{1}{2}\int_{\Omega} \dot{\boldsymbol{u}}^{\boldsymbol{T}} \boldsymbol{I}\dot{\boldsymbol{u}} \boldsymbol{d\Omega} \tag{30}$$

where $\mathbf{I}$ represents the inertia matrix, which contains all the relevant inertia terms as

$$\boldsymbol{I} = \begin{bmatrix} \boldsymbol{I_0} & \mathbf{0} & \mathbf{0} & \boldsymbol{I_1} & \mathbf{0} \\ \mathbf{0} & \boldsymbol{I_0} & \mathbf{0} & \mathbf{0} & \boldsymbol{I_1} \\ \mathbf{0} & \mathbf{0} & \boldsymbol{I_0} & \mathbf{0} & \mathbf{0} \\ \boldsymbol{I_1} & \mathbf{0} & \mathbf{0} & \boldsymbol{I_2} & \mathbf{0} \\ \mathbf{0} & \boldsymbol{I_1} & \mathbf{0} & \mathbf{0} & \boldsymbol{I_2} \end{bmatrix} \tag{31}$$

$$I_i = \int_{-h/2}^{h/2} \rho\, z^i dz, for\ i = 0,1,2 \tag{32}$$

3.3 Governing equation

The generalized displacements are independently interpolated using the MK shape function

$$\boldsymbol{u^h(x)} = \begin{Bmatrix} \boldsymbol{u_0} \\ \boldsymbol{v_0} \\ \boldsymbol{w_0} \\ \boldsymbol{\phi_x} \\ \boldsymbol{\phi_y} \end{Bmatrix} = \sum_{i=1}^{n} \boldsymbol{\varphi_i} \begin{Bmatrix} \widehat{\boldsymbol{u}} \\ \widehat{\boldsymbol{v}} \\ \widehat{\boldsymbol{w}} \\ \widehat{\boldsymbol{\phi}}_{\boldsymbol{x}} \\ \widehat{\boldsymbol{\phi}}_{\boldsymbol{y}} \end{Bmatrix} = \sum_{i=1}^{n} \boldsymbol{\varphi_i(x) u_i} \tag{33}$$

Now, the strain components can be obtained using the approximated displacements

$$\boldsymbol{\varepsilon_m} = \sum_{i=1}^{n} \boldsymbol{B_m u_i}\,; \boldsymbol{\varepsilon_b} = \sum_{i=1}^{n} \boldsymbol{B_b u_i}\,; \boldsymbol{\gamma_s} = \sum_{i=1}^{n} \boldsymbol{B_s u_i} \tag{34}$$

where $\mathbf{B}_m$, $\mathbf{B}_b$ and $\mathbf{B}_s$ are the strain-displacement matrices and are defined as

$$\boldsymbol{B_m} = \begin{bmatrix} \frac{\partial \boldsymbol{\varphi}}{\partial \boldsymbol{x}} & \mathbf{0} & \mathbf{0} & \mathbf{0} & \mathbf{0} \\ \mathbf{0} & \frac{\partial \boldsymbol{\varphi}}{\partial \boldsymbol{y}} & \mathbf{0} & \mathbf{0} & \mathbf{0} \\ \frac{\partial \boldsymbol{\varphi}}{\partial \boldsymbol{y}} & \frac{\partial \boldsymbol{\varphi}}{\partial \boldsymbol{x}} & \mathbf{0} & \mathbf{0} & \mathbf{0} \end{bmatrix} \tag{35}$$

$$\boldsymbol{B_b} = \begin{bmatrix} \mathbf{0} & \mathbf{0} & \mathbf{0} & \frac{\partial \boldsymbol{\varphi}}{\partial \boldsymbol{x}} & \mathbf{0} \\ \mathbf{0} & \mathbf{0} & \mathbf{0} & \mathbf{0} & \frac{\partial \boldsymbol{\varphi}}{\partial \boldsymbol{y}} \\ \mathbf{0} & \mathbf{0} & \mathbf{0} & \frac{\partial \boldsymbol{\varphi}}{\partial \boldsymbol{y}} & \frac{\partial \boldsymbol{\varphi}}{\partial \boldsymbol{x}} \end{bmatrix} \tag{36}$$

$$\boldsymbol{B_s} = \begin{bmatrix} \mathbf{0} & \mathbf{0} & \frac{\partial \boldsymbol{\varphi}}{\partial \boldsymbol{x}} & \boldsymbol{\varphi} & \mathbf{0} \\ \mathbf{0} & \mathbf{0} & \frac{\partial \boldsymbol{\varphi}}{\partial \boldsymbol{y}} & \mathbf{0} & \boldsymbol{\varphi} \end{bmatrix} \tag{37}$$

Substituting Eqs. (23), (26), (27), (30) into Eq. (22), after a number of simplifications, leads to the following coupled matrix equations:

$$\left[\left(\boldsymbol{K} + \boldsymbol{K_f} + \boldsymbol{N^0 K_G}\right) - \boldsymbol{\omega^2 M}\right]\overline{\boldsymbol{u}} = \mathbf{0} \tag{38}$$

Specifically for the above equation, for buckling analysis, $\omega = 0$, and for the case of free vibration analysis, $N^0 = 0$. $\mathbf{K}$ is the stiffness matrix, $\mathbf{M}$ is the mass matrix, $\mathbf{K}_G$ is the geometric stiffness matrix, $\overline{\mathbf{u}}$ is the eigenvector and ω is the natural vibration frequency of structure. These matrices can be calculated as

$$\boldsymbol{K} = \int_{\Omega} \begin{bmatrix} \boldsymbol{B_m} \\ \boldsymbol{B_b} \\ \boldsymbol{B_s} \end{bmatrix}^{\boldsymbol{T}} \begin{bmatrix} \boldsymbol{A} & \boldsymbol{B} & \mathbf{0} \\ \boldsymbol{B} & \boldsymbol{D} & \mathbf{0} \\ \mathbf{0} & \mathbf{0} & \boldsymbol{A_s} \end{bmatrix} \begin{bmatrix} \boldsymbol{B_m} \\ \boldsymbol{B_b} \\ \boldsymbol{B_s} \end{bmatrix} \boldsymbol{d\Omega} \tag{39}$$

$$\boldsymbol{K_f} = \int_{\Omega} \left(\boldsymbol{B_w}^{\boldsymbol{T}} \boldsymbol{k_1 B_w} - \boldsymbol{B_w}^{\boldsymbol{T}} \boldsymbol{k_2 B_f} \right) \boldsymbol{d\Omega} \tag{40}$$

$$\boldsymbol{B_w} = [\mathbf{0} \quad \mathbf{0} \quad \boldsymbol{\varphi} \quad \mathbf{0} \quad \mathbf{0}] \tag{41}$$

$$\boldsymbol{B_f} = \left[\mathbf{0} \quad \mathbf{0} \quad \left(\frac{\partial^2 \boldsymbol{\varphi}}{\partial \boldsymbol{x}^2} + \frac{\partial^2 \boldsymbol{\varphi}}{\partial \boldsymbol{y}^2}\right) \quad \mathbf{0} \quad \mathbf{0}\right] \tag{42}$$

$$\boldsymbol{K_G} = \int_{\Omega} \boldsymbol{B_g}^{\boldsymbol{T}} \boldsymbol{S}^{\mathbf{0}} \boldsymbol{B_g} \boldsymbol{d\Omega} \tag{43}$$

$$\boldsymbol{B_g} = \begin{bmatrix} \frac{\partial \varphi}{\partial x} & \frac{\partial \varphi}{\partial y} & 0 & 0 & 0 & 0 & 0 & 0 & 0 & 0 \\ 0 & 0 & \frac{\partial \varphi}{\partial x} & \frac{\partial \varphi}{\partial y} & 0 & 0 & 0 & 0 & 0 & 0 \\ 0 & 0 & 0 & 0 & \frac{\partial \varphi}{\partial x} & \frac{\partial \varphi}{\partial y} & 0 & 0 & 0 & 0 \\ 0 & 0 & 0 & 0 & 0 & 0 & \frac{\partial \varphi}{\partial x} & \frac{\partial \varphi}{\partial y} & 0 & 0 \\ 0 & 0 & 0 & 0 & 0 & 0 & 0 & 0 & \frac{\partial \varphi}{\partial x} & \frac{\partial \varphi}{\partial y} \end{bmatrix}^{\boldsymbol{T}} \tag{44}$$

$$\boldsymbol{S}^{\mathbf{0}} = \begin{bmatrix} h\hat{\sigma}_0 & 0 & 0 & 0 & 0 \\ 0 & h\hat{\sigma}_0 & 0 & 0 & 0 \\ 0 & 0 & h\hat{\sigma}_0 & 0 & 0 \\ 0 & 0 & 0 & \frac{h^3}{12}\hat{\sigma}_0 & 0 \\ 0 & 0 & 0 & 0 & \frac{h^3}{12}\hat{\sigma}_0 \end{bmatrix} \tag{45}$$

$$\boldsymbol{M} = \boldsymbol{B_M^T I B_M} \tag{46}$$

$$\boldsymbol{B_M} = \begin{bmatrix} \varphi & 0 & 0 & 0 & 0 \\ 0 & \varphi & 0 & 0 & 0 \\ 0 & 0 & \varphi & 0 & 0 \\ 0 & 0 & 0 & \varphi & 0 \\ 0 & 0 & 0 & 0 & \varphi \end{bmatrix} \tag{47}$$

For numerical integration, we employ a background cell consisting of 2×2 Gaussian points. Furthermore, the Kronecker's delta property of the MK shape function allows for a straightforward implementation of BC, similar to conventional FEM. Here are the details of the BC used in the analyses:

Clamped support (C): $u_0 = v_0 = w_0 = \theta_x = \theta_y = 0$ at the entire edge.

Simply support (S): $u_0 = w_0 = \theta_x = 0$ at $y = 0$ & $y = W$; $v_0 = w_0 = \theta_y = 0$ at $x = 0$ & $x = L$.

4 NUMERICAL RESULTS

In this section, the effectiveness and accuracy of the present meshfree method are investigated. Examples of buckling and free vibration analysis of laminated composite plates are performed, further verified in the presence of a PF. The considered laminated composite plates have layers of equal thickness and each layer is made of the same orthotropic material. Next, research problems on the critical buckling load and natural frequency of bio-inspired helicoid laminated composite plates will be conducted. The effects of thickness, PF parameters, and layer scheme will be investigated and discussed, along with figures illustrating the eigenmode shapes of square plates and plates with heart-shaped holes. We use the scale parameter of the support domain as $\alpha = 2$ in the analysis.

The obtained critical buckling load and natural frequency are presented in non-dimensional forms as $N^n = N^0 \frac{b^2}{E_{22}h^3}$, $\omega^n = \omega \frac{b^2}{h}\sqrt{\frac{\rho}{E_{22}}}$. In addition, the two stiffness parameters of the Pasternak elastic foundation are also expressed in non-dimensional forms: $K_1 = \frac{k_1 L^4}{E_{22}h^3}$, $K_2 = \frac{k_2 L^2}{E_{22}h^3}$

4.1 Verification

First, the validation of the present meshfree method will begin with an example of buckling analysis of a square cross-ply laminated composite plate. Each layer of the plate is made of an orthotropic material with the following properties: $E_{11}/E_{22} = open, G_{12} = G_{13} = 0.6E_{22}, G_{23} = 0.5E_{22}, \nu_{12} = 0.25$. The plate has a thickness of $a/h = 10$ and is subjected to simply supported BC. The results are shown in Table 2. Next, the natural frequencies of a fully clamped square angle-ply plate with thickness ratio $a/h = 100$ and material properties $E_{11}/E_{22} = 25, G_{12} = G_{13} = 0.5E_{22}, G_{23} = 0.2E_{22}, \nu_{12} = 0.25, \rho = 1300$ are also investigated as given in Table 3. In both examples, uniform node distributions are gradually increased from 5×5 to 17×17 and the results obtained show good convergence and agree well with previously published results. To ensure the accuracy of subsequent problems, a node distribution of 17×17 will be used.

Table 2 Non-dimensional critical buckling loads of SSSS cross-ply laminated composite plate, $a/h = 10$.

Layup	E_{11}/E_{22}	Present				Ref-1	Ref-2	Noor (1975)
		5×5	9×9	13×13	17×17			
$0/90/0$	20	15.481	14.709	14.645	14.618	15.003	14.985	15.019
	30	19.606	18.596	18.518	18.489	19.002	19.027	19.304
	40	22.960	21.734	21.645	21.616	22.330	22.315	22.880
$0/90/0/90/0$	20	16.361	15.590	15.520	15.490	15.828	15.736	15.653
	30	21.297	20.277	20.188	20.152	20.643	20.485	20.466
	40	25.537	24.279	24.176	24.137	24.756	24.547	24.593

Note that: Ref-1: Sayyad and Ghugal (2014) using their sinusoidal shear and normal deformation theory (SSNDT). Ref-2: Sayyad and Ghugal (2014) using first order shear deformation theory (FSDT) of Mindlin (1951)

Table 3 Non-dimensional natural frequencies of CCCC angle-ply laminated composite plate, $a/h = 100$.

Layup	Mode number	Present				Zhang et al. (2018)	Qin et al. (2019)
		5×5	9×9	13×13	17×17		
$15/-15/15/-15$	1	32.072	30.258	30.516	30.499	30.924	30.939
	2	42.384	39.154	39.705	39.574	40.138	40.012
	3	77.905	54.547	55.428	55.184	55.906	55.708
	4	108.813	75.420	76.994	77.123	78.279	77.925
	5	403.565	80.175	78.122	77.442	79.524	79.219
	6	421.889	83.860	86.527	86.310	89.019	88.515
$30/-30/30/-30$	1	30.560	29.208	29.586	29.584	29.818	29.772
	2	50.834	46.480	47.488	47.450	47.996	47.762
	3	71.033	67.379	68.902	69.006	70.056	69.718
	4	113.424	72.164	73.585	73.472	74.436	73.877
	5	450.549	87.157	90.254	90.122	91.737	91.031
	6	473.404	111.558	108.330	107.583	108.905	108.095
$45/-45/45/-45$	1	29.955	28.876	29.318	29.321	29.487	29.279
	2	61.532	56.981	58.359	58.407	58.940	58.553
	3	61.532	56.981	58.359	58.407	58.940	58.553
	4	116.090	89.158	92.530	92.447	93.641	92.858
	5	498.605	97.396	99.442	99.497	100.720	99.934
	6	519.665	98.302	100.055	100.120	101.021	100.665

In the next example, a two cross-ply square laminated composite plate resting on a PF is considered with simply supported BC, thickness $a/h = 10$. The orthotropic material properties used are: $E_{11}/E_{22} = \text{open}, G_{12} = G_{13} = 0.6E_{22}, G_{23} = 0.5E_{22}, \nu_{12} = 0.25, \rho = 100$. The cases of E_{11}/E_{22} ratio are considered for results in agreement with Setoodeh et al. Setoodeh and Karami (2004) using the 3-D Layer-wise FEM method as shown in Table 4. Table 5 shows the non-dimensional natural frequencies of vibration of the cross-ply laminated composite plate $0/90/0$. The plate is placed on a PF with simply supported BC, $E_{11}/E_{22} = 40$. Through the cases of thickness ratio, the obtained results are in good agreement with Shen et al. Shen, Zheng and Huang (2003) using Reddy's Higher order-SDT and Akavci Akavci (2007) using Hyperbolic-SDT. Through the examples performed above, the effectiveness and accuracy of the present meshfree method have been verified.

Table 4 Non-dimensional critical buckling loads of SSSS two cross-ply laminated composite plate resting on PF, $a/h = 10$.

(K_1, K_2)	Source	E_{11}/E_{22} 20	30	40
(0,0)	Present	7.871	9.532	11.123
	Noor (1975)	7.820	9.375	10.817
	Reddy and Khdeir (1989)	8.042	9.735	11.353
	Setoodeh and Karami (2004)	8.046	9.700	11.238
(100,0)	Present	14.530	16.925	19.047
	Setoodeh and Karami (2004)	15.325	17.525	19.340
(100,10)	Present	26.487	28.931	31.099
	Setoodeh and Karami (2004)	27.535	29.762	31.598

Table 5 Non-dimensional natural frequencies of SSSS $0/90/0$ laminated composite plate resting on PF.

(K_1, K_2)	Source	a/h 10	20	50
(0,0)	Present	14.616	17.461	18.654
	Shen, Zheng and Huang (2003)	14.702	17.483	18.689
	Akavci (2007)	14.700	17.481	18.640
(100,0)	Present	17.681	20.113	21.164
	Shen, Zheng and Huang (2003)	17.753	20.132	21.152
	Akavci (2007)	17.751	20.131	21.152
(100,10)	Present	22.561	24.538	25.416
	Shen, Zheng and Huang (2003)	22.596	24.536	25.390
	Akavci (2007)	22.595	24.535	25.390

Table 6 Non-dimensional critical buckling loads of 16 layers SCSC BiHLC plate resting on PF via layup scheme, thickness ratio a/h and foundation parameter (K_1, K_2).

a/h	(K_1, K_2)	HR			HE			HS		
		Type 1	Type 2	Type 3	Type 1	Type 2	Type 3	Type 1	Type 2	Type 3
15	(0,0)	47.8751	47.7691	47.9744	46.0048	44.7404	49.3440	41.6269	46.3070	49.5164
	(50,0)	51.2457	51.0575	51.1379	49.3027	47.7239	51.8513	44.3949	48.3169	51.5691
	(0,25)	86.9747	87.2473	87.4733	85.7043	84.4737	85.0181	81.5098	78.0252	81.7424
	(50,25)	88.7473	89.0305	89.2221	87.4639	86.0923	85.9767	82.5193	78.9364	82.6549
25	(0,0)	67.1543	66.2191	65.5723	64.4842	61.2341	65.1359	55.0501	60.5951	65.5309
	(50,0)	70.8134	69.8240	69.0980	68.0899	64.6058	68.3263	58.1534	63.1866	68.4030
	(0,25)	110.6627	109.9793	109.5036	108.4660	105.5441	107.8691	99.4903	97.4083	105.5235
	(50,25)	113.8308	113.1141	112.5671	111.6051	108.4627	110.4559	102.1225	98.3856	107.4740
40	(0,0)	78.2675	76.7369	75.4397	75.3305	70.6863	73.3047	62.5755	67.7743	73.3571
	(50,0)	81.9951	80.4214	79.0624	79.0132	74.1746	76.6821	65.7841	70.5911	76.5008
	(0,25)	122.8051	121.4967	120.4544	120.2781	116.1173	118.1281	108.2783	108.5645	116.1439
	(50,25)	126.3061	124.9596	123.8538	123.7451	119.3896	121.1797	111.2429	109.5563	118.8125
75	(0,0)	84.8563	83.0115	81.3106	82.0209	76.5033	78.0580	67.2930	71.7222	77.6293
	(50,0)	88.6083	86.7209	84.9646	85.7206	80.0271	81.4984	70.5304	74.6429	80.8849
	(0,25)	129.7777	128.1238	126.7103	127.2682	122.2953	123.6974	113.4129	114.3659	121.7039
	(50,25)	133.3939	131.6987	130.2262	130.8402	125.6890	126.9209	116.4946	116.2632	124.6095

Table 7 Non-dimensional critical buckling loads of 28 layers CCCC BiHLC plate resting on PF via layup scheme, thickness ratio a/h and foundation parameter (K_1, K_2).

a/h	(K_1, K_2)	HR			HE			HS		
		Type 1	Type 2	Type 3	Type 1	Type 2	Type 3	Type 1	Type 2	Type 3
20	(0,0)	59.3070	59.9869	61.2326	62.2910	59.2125	56.6020	47.8932	49.2304	59.1975
	(40,0)	61.9704	62.4930	63.6919	64.8258	61.3153	58.7330	49.9579	50.8589	61.0452
	(0,5)	68.2948	68.7332	69.7983	70.8256	67.3404	65.0814	56.9189	56.8743	66.6982
	(40,5)	70.8545	71.1201	72.1285	73.2218	69.3040	67.0917	58.9033	58.2779	68.3761
30	(0,0)	70.8626	70.4314	71.3277	72.7666	68.6290	65.8574	56.1443	57.1636	69.3654
	(40,0)	73.6649	73.1241	73.9994	75.5122	71.0207	68.2418	58.3616	58.9959	71.5741
	(0,5)	80.0295	79.4995	80.2850	81.6893	77.3003	74.7920	65.4216	65.2868	77.5173
	(40,5)	82.7855	82.1361	82.8934	84.3687	79.6117	77.1129	67.6037	67.0057	79.6072
50	(0,0)	78.8322	77.4357	77.9626	79.6966	74.6253	71.8836	61.7306	62.4197	75.9111
	(40,0)	81.7007	80.2161	80.7314	82.5336	77.1608	74.3963	64.0379	64.3753	78.3132
	(0,5)	88.0820	86.6599	87.1137	88.8044	83.5929	81.0562	71.1446	70.8564	84.4509
	(40,5)	90.9258	89.4086	89.8453	91.6031	86.0757	83.5302	73.4356	72.7193	86.7662

Table 7 Continued...

a/h	(K_1, K_2)	HR			HE			HS		
		Type 1	Type 2	Type 3	Type 1	Type 2	Type 3	Type 1	Type 2	Type 3
75	(0,0)	81.7246	79.9439	80.3162	82.1654	76.7161	74.0094	63.7412	64.2932	78.2075
	(40,0)	84.6131	82.7508	83.1139	85.0290	79.2955	76.5620	66.0787	66.2906	80.6701
	(0,5)	91.0000	89.2169	89.5281	91.3306	85.7798	83.2581	73.2008	72.8411	86.8770
	(40,5)	93.8696	91.9987	92.2957	94.1632	88.3145	85.7789	75.5273	74.7527	89.2629

Table 8 Non-dimensional critical buckling loads of SSSS BiHLC plate resting on PF via NOL, $a/h = 30$.

NOL	(K_1, K_2)	HR			HE			HS		
		Type 1	Type 2	Type 3	Type 1	Type 2	Type 3	Type 1	Type 2	Type 3
12	(0,0)	22.7214	23.0400	23.4338	22.6173	22.8809	23.5624	25.4329	25.3748	24.7480
	(30,0)	25.7502	26.0624	26.4472	25.6344	25.8745	26.5173	28.3273	28.3273	27.7014
	(0,15)	52.7655	53.0861	53.4840	52.6640	52.9360	53.6357	55.5191	55.4175	54.7988
	(30,15)	55.7944	56.1086	56.4976	55.6813	55.9303	56.5923	58.4139	58.3675	57.7511
16	(0,0)	22.9480	23.6127	24.0622	22.8854	23.9813	23.6495	24.8025	25.3930	25.5633
	(30,0)	25.9718	26.6195	27.0520	25.8849	26.9247	26.6087	27.6545	28.3073	28.5303
	(0,15)	52.9935	53.6661	54.1237	52.9383	54.0601	53.6895	54.8936	55.4095	55.5967
	(30,15)	56.0174	56.6732	57.1139	55.9383	57.0048	56.6480	57.7467	58.3161	58.5620
20	(0,0)	23.3183	24.0769	24.5289	23.6688	25.3113	23.8063	24.2804	25.1640	26.8026
	(30,0)	26.3328	27.0637	27.5028	26.6350	28.2996	26.7329	27.1020	28.0443	29.7837
	(0,15)	53.3677	54.1391	54.5873	53.7380	55.3455	53.8435	54.3776	55.1479	56.8301
	(30,15)	56.3824	57.1264	57.5613	56.7054	58.3332	56.7682	57.2010	58.0127	59.8094
24	(0,0)	23.7312	24.4413	25.3568	23.8301	25.4530	23.6278	23.8719	24.9590	27.9120
	(30,0)	26.7325	27.4147	28.3328	26.7721	28.4188	26.5582	26.6716	27.8047	30.9035
	(0,15)	53.7874	54.5009	55.4055	53.8970	55.4865	53.6682	53.9757	54.9420	57.9383
	(30,15)	56.7890	57.4745	58.3812	56.8392	58.4511	56.5971	56.7780	57.7714	60.9281
28	(0,0)	24.0388	25.0833	26.1737	27.5240	25.2635	23.6256	23.5777	24.6791	28.4362
	(30,0)	27.0255	28.0565	29.1564	30.5293	28.2156	26.5330	26.3556	27.5056	31.4304
	(0,15)	54.1011	55.1343	56.2172	57.5646	55.2932	53.6626	53.6851	54.6288	58.4618
	(30,15)	57.0882	58.1073	59.1994	60.5696	58.2432	56.5681	56.4659	57.4301	61.4544

4.2 Buckling analysis of BiHLC plate

Henceforth, all BiHLC plates will be made of an orthotropic material with the following properties: $E_{11}/E_{22} = 25, G_{12} = G_{13} = 0.6E_{22}, G_{23} = 0.5E_{22}, \nu_{12} = 0.25, \rho = 100$.

First, to investigate the effect of helicoidal scheme on the critical buckling load, we consider square BiHLC plates resting on a Pasternak elastic foundation. The problems are solved for various thickness parameters and elastic foundation parameters. Table 6 presents the results for the SCSC boundary condition and Table 7 for the CCCC boundary condition. It is observed that the BiHLC plate type can significantly affect the critical buckling load. Specifically, the largest difference occurs for the CCCC boundary condition, thickness $a/h = 20$, $(K_1, K_2) = (0,0)$, the critical buckling load of the HE type 1 is 30.06% higher than that of the HS type 1. It can be seen that because the orthotropic material has different properties in two directions, the choice of an appropriate helicoidal scheme can greatly affect the bending resistance of the BiHLC plate under uniaxial load. In addition, as expected, a smaller plate thickness reduces the stiffness of the plate, but the critical buckling load increases due to the non-dimensional formula used. Furthermore, parameter K_2 plays a more important role than K_1 for the critical buckling load.

Table 8 presents the effect of NOL on the non-dimensional critical buckling load of the BiHLC plate. From the obtained results, no clear trend can be drawn. Although the change of NOL still has a great impact on the critical buckling load, the increase or decrease of the impact depends on the helicoidal scheme used. Specifically, the majority of the helicoidal schemes show a non-dimensional critical buckling load that is monotonically increasing with NOL, while the HS type 1 plate shows an inverse relationship, and the HE type 2, HE type 3, HS type 2 plates show non-monotonic behavior.

Next, a square HE type 3 SSSS BiHLC plate with thickness ratio $a/h = 30$ and resting on a Pasternak elastic foundation is considered. The two stiffness parameters of the foundation used are $K_1 = 100$ and $K_2 = 10$. Figure 3 shows the first six eigenmode shapes of the buckling analysis and the corresponding six nondimensional buckling loads. Unlike symmetrically plates, the mode shapes shown in Figure 1 do not exhibit any similar mode shapes, which is a consequence of uniaxial compression and lay-up scheme of the BiHLC plate.

Finally, to illustrate the applicability of the meshfree method being used for structures with complex geometries, consider a 12 layers HR type 1 BiHLC plate with a heart-shaped hole (see geometric dimension in Figure 4) resting on PF.

The plate has thickness ratio $a/h = 45$ and $(K_1, K_2) = (35,5)$. Figure 5 presents the first six eigenmode shapes of the buckling analysis and the corresponding non-dimensional critical buckling loads.

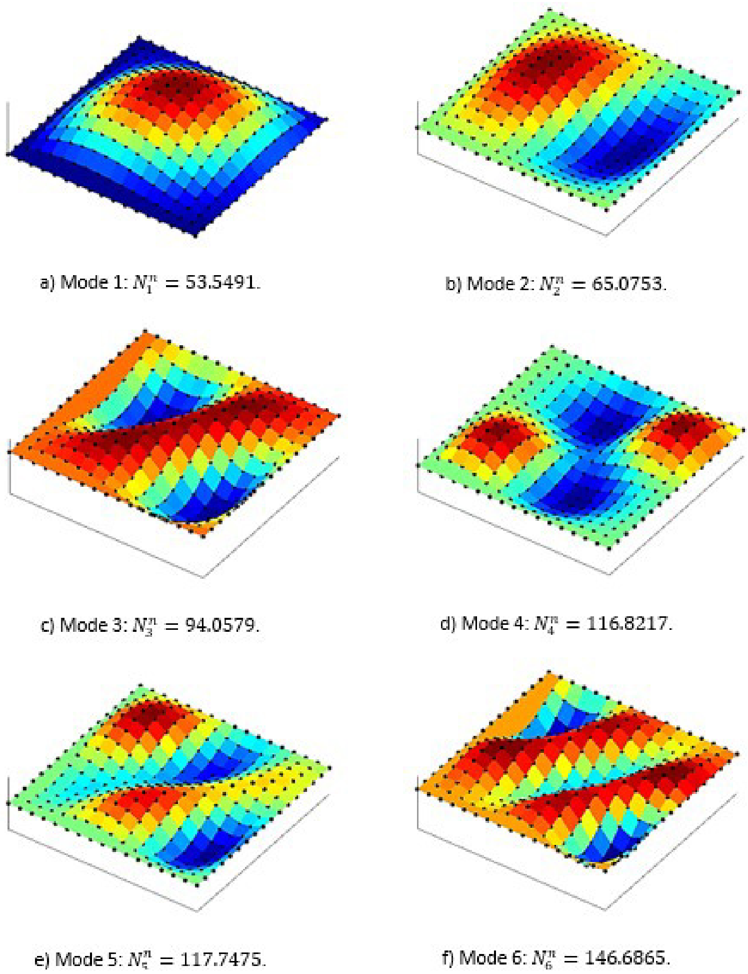

Figure 3. Six lowest non-dimensional eigenmode shapes for buckling analysis of HE type 3 SSSS BiHLC plate resting on PF, $a/h = 30$, $(K_1, K_2) = (100,10)$.

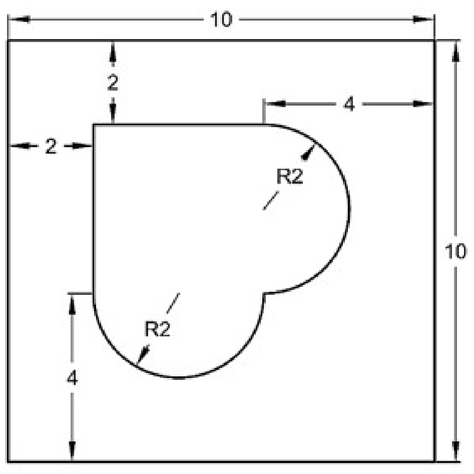

Figure 4. The model of BiHLC plate with a heart-shaped hole.

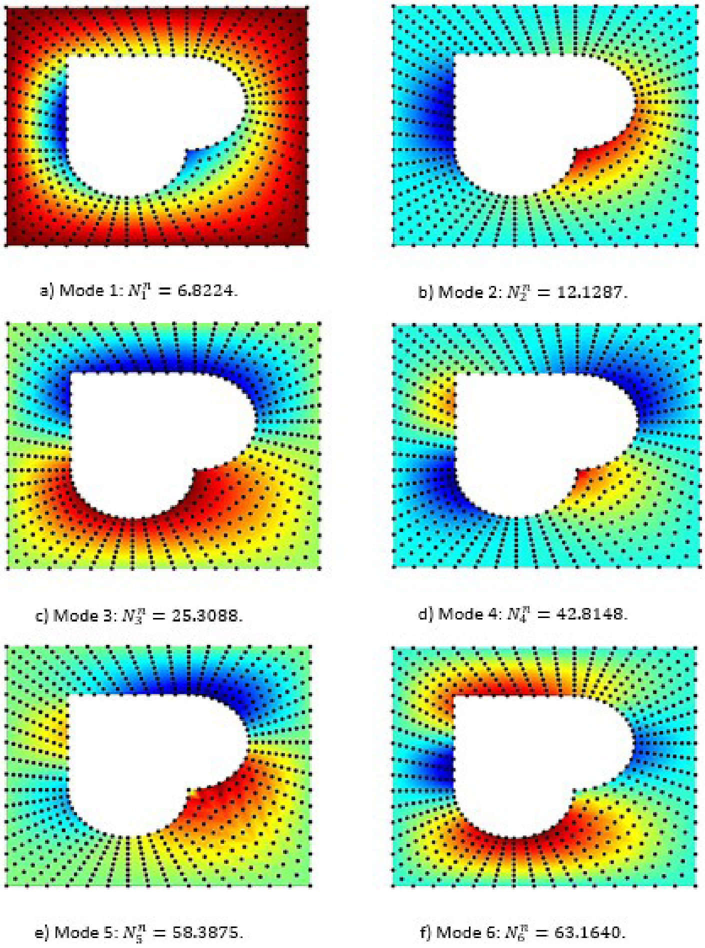

Figure 5. Six lowest non-dimensional eigenmode shapes for buckling analysis of HR type 1 SSSS BiHLC plate with a heart-shaped hole resting on PF, $a/h = 45$, $(K_1, K_2) = (35,5)$.

4.3 Free vibration analysis of BiHLC plate

In this section, the factors affecting the natural vibration frequency of BiHLC plates will be investigated in turn. First, Tables 9 and 10 present the first natural frequency of various BiHLC plate type with different thickness and foundation parameter cases. Table 9 presents the SCSC boundary condition, while Table 10 presents the CCCC condition. In almost all helicoidal schemes, H-s1 gives the smallest first natural frequency, except in the case of SCSC boundary condition, $a/h = 15$, $(K_1, K_2) = (0,25)$ and $(50,25)$, HE type 1 gives the smallest first natural frequency. The effects of thickness and foundation parameter are also similar to those mentioned in the buckling analysis.

Table 9 Non-dimensional natural frequencies of 16 layers SCSC BiHLC plate resting on PF via layup scheme, thickness ratio a/h and foundation parameter (K_1, K_2).

a/h	(K_1, K_2)	HR			HE			HS		
		Type 1	Type 2	Type 3	Type 1	Type 2	Type 3	Type 1	Type 2	Type 3
15	(0,0)	23.3759	23.4840	23.7363	23.0313	23.1873	24.9354	22.8878	25.4468	25.7571
	(50,0)	24.4168	24.5203	24.7620	24.0870	24.2362	25.9142	23.9496	26.4068	26.7061
	(0,25)	32.6894	32.7832	33.0037	32.4528	32.6425	33.9416	32.5088	34.3405	34.5264
	(50,25)	33.4421	33.5338	33.7493	33.2108	33.3962	34.6674	33.2653	35.0581	35.2403
25	(0,0)	28.3555	28.2482	28.2637	27.8406	27.5451	28.7256	26.6747	28.9527	29.3770
	(50,0)	29.2219	29.1178	29.1327	28.7224	28.4361	29.5811	27.5936	29.8016	30.2141
	(0,25)	36.6696	36.6060	36.6720	36.2761	36.1561	37.1796	35.6116	37.4338	37.6956
	(50,25)	37.3437	37.2812	37.3460	36.9573	36.8395	37.8445	36.3052	38.0943	38.3517
40	(0,0)	31.4993	31.2383	30.6822	30.5043	29.9151	30.6669	28.7094	30.6120	31.1083
	(50,0)	31.8591	31.6234	31.4856	31.3122	30.7385	31.4706	29.5664	31.4172	31.9009
	(0,25)	38.9924	38.8160	38.7591	38.5461	38.1916	38.9293	37.3792	38.9906	39.3027
	(50,25)	39.6278	39.4542	39.3982	39.1886	38.8400	39.5656	38.0414	39.6260	39.9331

Table 9 Continued...

a/h	(K_1, K_2)	HR			HE			HS		
		Type 1	Type 2	Type 3	Type 1	Type 2	Type 3	Type 1	Type 2	Type 3
75	(0,0)	32.6452	32.3518	32.1241	32.1540	31.3957	31.8508	30.0323	31.5230	32.0770
	(50,0)	33.4019	33.1153	32.8929	32.9221	32.1818	32.6260	30.8532	32.3060	32.8469
	(0,25)	40.3938	40.1725	40.0439	40.0039	39.5063	40.0247	38.5636	39.8703	40.2269
	(50,25)	41.0079	40.7898	40.6632	40.6238	40.1339	40.6443	39.2063	40.4922	40.8434

Table 10 Non-dimensional natural frequencies of 28 layers CCCC BiHLC plate resting on PF via layup scheme, thickness ratio a/h and foundation parameter (K_1, K_2).

a/h	(K_1, K_2)	HR			HE			HS		
		Type 1	Type 2	Type 3	Type 1	Type 2	Type 3	Type 1	Type 2	Type 3
20	(0,0)	26.8828	27.3766	27.7414	27.7229	28.1438	27.5393	25.7608	27.1203	28.4768
	(40,0)	27.6143	28.0953	28.4509	28.4330	28.8435	28.2538	26.5230	27.8455	29.1686
	(0,5)	28.8746	29.3458	29.6797	29.6457	30.0723	29.5328	27.9279	29.1606	30.3571
	(40,5)	29.5569	30.0174	30.3440	30.3108	30.7281	30.2002	28.6326	29.8363	31.0070
30	(0,0)	29.7654	29.9492	30.1712	30.2285	30.2999	29.8019	28.1465	29.1692	30.6035
	(40,0)	30.4287	30.6086	30.8258	30.8819	30.9517	30.4644	28.8469	29.8457	31.2491
	(0,5)	31.6237	31.8151	32.0200	32.0552	32.1649	31.7201	30.2107	31.1512	32.4221
	(40,5)	32.2489	32.4365	32.6376	32.6721	32.7797	32.3434	30.8644	31.7856	33.0321
50	(0,0)	31.6918	31.6347	31.7412	31.8631	31.6438	31.2401	29.6974	30.4527	31.9271
	(40,0)	32.3163	32.2603	32.3647	32.4843	32.2692	31.8734	30.3628	31.1020	32.5470
	(0,5)	33.4801	33.4474	33.5451	33.6410	33.4799	33.1219	31.7098	32.4094	33.7175
	(40,5)	34.0718	34.0397	34.1357	34.2299	34.0716	33.7199	32.3339	33.0203	34.3051
75	(0,0)	32.3809	32.2317	32.2935	32.4414	32.1079	31.7416	30.2451	30.8984	32.3849
	(40,0)	32.9926	32.8461	32.9068	33.0520	32.7246	32.3653	30.8991	31.5388	32.9964
	(0,5)	34.1474	34.0281	34.0839	34.2044	33.9358	33.6127	32.2420	32.8482	34.1673
	(40,5)	34.7280	34.6107	34.6655	34.7841	34.5199	34.2023	32.8563	33.4513	34.7475

Table 11 Non-dimensional natural frequencies of SSSS BiHLC plate resting on PF via NOL, $a/h = 30$.

NOL	(K_1, K_2)	HR			HE			HS		
		Type 1	Type 2	Type 3	Type 1	Type 2	Type 3	Type 1	Type 2	Type 3
12	(0,0)	14.9874	15.1041	15.2494	14.9745	15.1050	15.4011	16.1203	15.9889	15.7888
	(30,0)	15.9553	16.0649	16.2016	15.9431	16.0658	16.3445	17.0238	16.8995	16.7103
	(0,15)	22.8378	22.9210	23.0264	22.8408	22.9499	23.1847	23.7302	23.5834	23.4477
	(30,15)	23.4843	23.5652	23.6677	23.4872	23.5933	23.8218	24.3531	24.2100	24.0778
16	(0,0)	15.0713	15.3199	15.4979	15.0957	15.5598	15.4233	16.0003	16.0683	16.0199
	(30,0)	16.0341	16.2680	16.4357	16.0570	16.4941	16.3653	16.9102	16.9746	16.9288
	(0,15)	22.8980	23.0800	23.2167	22.9380	23.3037	23.1942	23.6846	23.6703	23.5886
	(30,15)	23.5429	23.7200	23.8530	23.5817	23.9376	23.8311	24.3086	24.2947	24.2151
20	(0,0)	15.2099	15.5083	15.6785	15.4149	15.8987	15.5368	15.8885	16.0592	16.3749
	(30,0)	16.1644	16.4455	16.6061	16.3574	16.8142	16.4724	16.8045	16.9660	17.2652
	(0,15)	22.9990	23.2267	23.3532	23.1834	23.4849	23.3017	23.6340	23.6913	23.8172
	(30,15)	23.6411	23.8627	23.9858	23.8206	24.1140	23.9356	24.2593	24.3152	24.4379
24	(0,0)	15.3691	15.6514	15.9370	15.5141	15.9878	15.4712	15.7952	16.0187	16.6889
	(30,0)	16.3143	16.5806	16.8504	16.4510	16.8985	16.4106	16.7162	16.9276	17.5632
	(0,15)	23.1186	23.3356	23.5247	23.2745	23.5677	23.2544	23.5887	23.6872	24.0242
	(30,15)	23.7575	23.9687	24.1529	23.9092	24.1947	23.8896	24.2151	24.3112	24.6396
28	(0,0)	15.4962	15.8561	16.1786	16.5441	15.9551	15.5141	15.7381	15.9791	16.8391
	(30,0)	16.4341	16.7739	17.0791	17.4257	16.8675	16.4510	16.6624	16.8902	17.7060
	(0,15)	23.2187	23.4728	23.6825	23.9114	23.5586	23.3040	23.5679	23.6706	24.1262
	(30,15)	23.8549	24.1023	24.3065	24.5296	24.1858	23.9379	24.1949	24.2949	24.7391

Continuing, Table 11 presents the effect of NOL on the non-dimensional natural frequencies. Plates HE type 2, HE type 3, and HS type 2 continue to show a non-monotonic variation of frequency with the change of NOL, while for plate HS type 1, increasing NOL lead to a decrease in non-dimensional frequency. It can be concluded that there is no direct relationship between NOL and non-dimensional natural frequency.

Next, a square HE type 3 BiHLC plate with SSSS BC is considered to be placed on an elastic foundation with parameters $K_1 = 100$ and $K_2 = 10$, thickness $a/h = 30$. The six lowest eigenmode shapes are presented in Figure 6 along with their corresponding non-dimensional natural frequencies. It can be observed that the second and third mode shapes have the same shape, however, their corresponding frequencies differ. This is due to the arrangement of the layers of the BiHLC plate, which makes one bending direction better than the other.

Finally, an HR type 1 SSSS BiHLC plate with thickness $a/h = 45$ is considered. The plate is rested on an elastic foundation with $K_1 = 35$ and $K_2 = 5$. To demonstrate the applicability of the meshfree method for free vibration analysis of plates with complex geometries, Figure 7 shows the first six eigenmode shapes along with the corresponding natural frequencies.

In this study, a MATLAB program was developed to perform the calculations, using floating-point numbers in double precision for higher accuracy. Since the stiffness, mass, and geometric stiffness at the integration points are independent of each other, they were computed in parallel across all CPU cores. The Intel(R) Core(TM) i5-9300H processor used in this study has 4 cores and 8 threads, which allowed the MATLAB simulations to efficiently utilize multi-threading. The system was equipped with 16.0 GB of RAM, operating at a speed of 2667 MHz with a CAS latency of 19 clocks. The analysis time for the buckling analysis and free vibration of the BiHLC plate with a heart-hole model with 600 nodes was approximately 22 seconds.

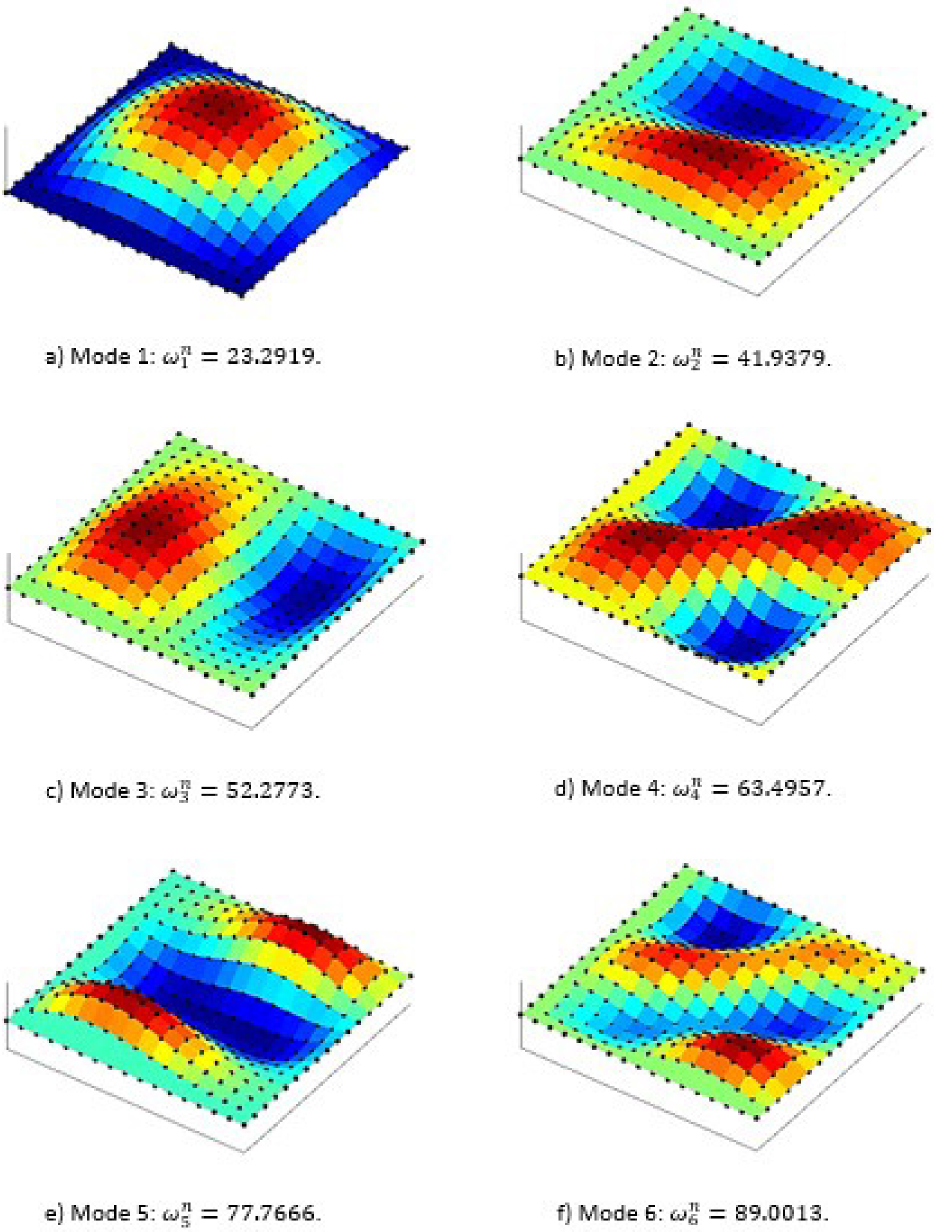

Figure 6 Six lowest non-dimensional eigenmode shapes for vibration analysis of HE type 3 SSSS BiHLC plate resting on PF, $a/h = 30$, $(K_1, K_2) = (100,10)$.

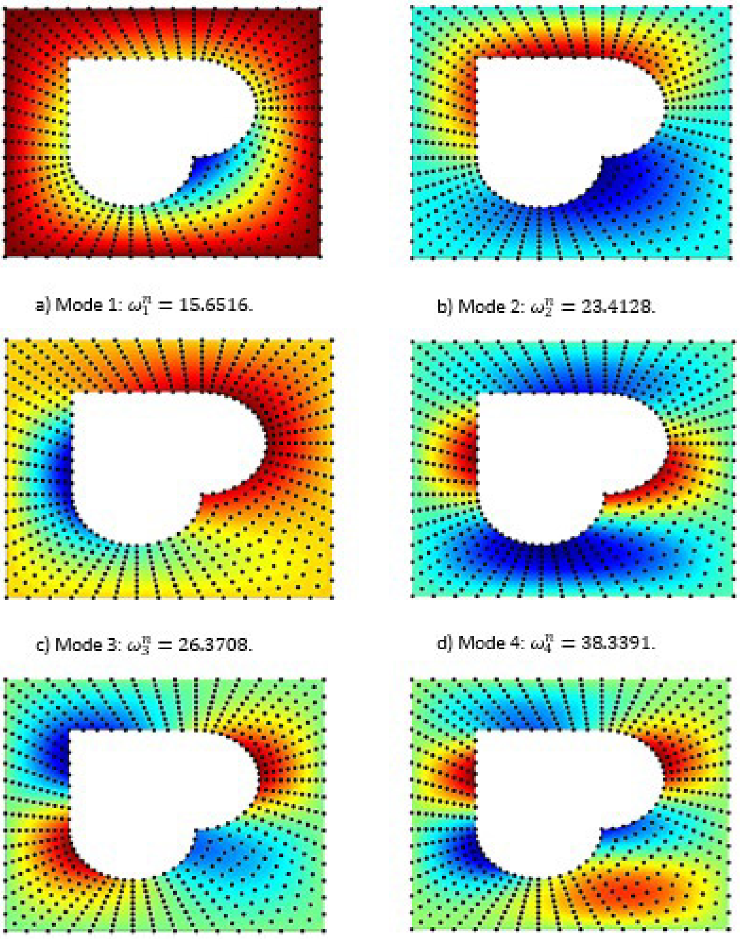

a) Mode 1: $\omega_1^n = 15.6516$. b) Mode 2: $\omega_2^n = 23.4128$.

c) Mode 3: $\omega_3^n = 26.3708$. d) Mode 4: $\omega_4^n = 38.3391$.

e) Mode 5: $\omega_5^n = 46.3849$. f) Mode 6: $\omega_6^n = 59.6440$.

Figure 7 Six lowest non-dimensional eigenmode shapes for vibration analysis of HR type 1 SSSS BiHLC plate with a heart-shaped hole resting on PF, $a/h = 45$, $(K_1, K_2) = (35,5)$.

5 CONCLUSIONS

This study focuses on the buckling and free vibration analysis of BiHLC plates with varying helicoidal configurations. The work is performed using the MK method based on Reddy's FSDT within the framework of Hamilton's principle. The accuracy of the present model is validated by comparing the obtained results with existing literature. A comprehensive investigation is conducted to explore the influence of the helicoidal layup scheme, geometrical properties, BCs, and the stiffness parameters of the PF. Key findings from this study are summarized as follows:

For buckling analysis, the critical buckling load of BiHLC plates is significantly affected by the choice of the helicoidal scheme, especially for certain BC and thickness ratios. The non-dimensional buckling load generally increases with decreasing plate thickness but can be counter-intuitive due to the formula used. Parameter K_2 of the PF has a stronger influence on the critical buckling load compared to K_1. The NOL can have a complex effect on the critical buckling load, depending on the specific helicoidal scheme.

For free vibration analysis, the first natural frequency of BiHLC plates is also dependent on the chosen helicoidal scheme. In most cases, the HS type 1 scheme results in the lowest frequency. Similar to buckling analysis, thickness and foundation parameters have predictable effects on the natural frequencies. There is no clear relationship between the number of layers and the natural frequency. Some schemes show an increase, some a decrease, and some non-monotonic behavior.

The study also demonstrates the meshfree MK method's applicability for analyzing plates with complex geometries, like a heart-shaped hole.

The power-law index increases reduce the FGS nanoplate stiffness, leading to a decrease in the These numerical results are anticipated to be instrumental in the design and manufacturing of composite plates used in critical structures like vehicles, submarines, turbine blades for wind and hydraulic applications, etc.

Author's Contributions: Investigation, Writing Original draft, Thanh Son Doan; Methodology, Validation, Formal analysis, Trung Thanh Tran; Conceptualization, Software, Huy Gia Luong; Writing - Reviewing & Editing, Supervision, Project administration, Pham Hong Thao; Writing Original draft, Software, Ngoc-Tu Do.

Editor: Marco L. Bittencourt

References

Adim, B. and T. Hassaine Daouadji (2023). Free Vibration Behavior of Laminated Composite Plates. *International Conference on Vibration Problems*, Springer.

Akavci, S. S. (2007). "Buckling and Free Vibration Analysis of Symmetric and Antisymmetric Laminated Composite Plates on an Elastic Foundation." *Journal of Reinforced Plastics and Composites - J REINF PLAST COMPOSITE 26*: 1907-1919.

Bakoura, A., et al. (2022). "A mechanical behavior of composite plates using a simple three variable refined plate theory." *Structural Engineering and Mechanics 83*(5): 617.

Bui, T. Q. and M. N. Nguyen (2013). "Meshfree Galerkin Kriging model for bending and buckling analysis of simply supported laminated composite plates." *International Journal of Computational Methods 10*(03): 1350011.

Bui, T. Q., et al. (2018). "Analysis of transient dynamic fracture parameters of cracked functionally graded composites by improved meshfree methods." *Theoretical and Applied Fracture Mechanics 96*: 642-657.

Bui, T. Q., T. N. Nguyen and H. Nguyen-Dang (2009). "A moving Kriging interpolation-based meshless method for numerical simulation of Kirchhoff plate problems." *International journal for numerical methods in engineering 77*(10): 1371-1395.

Cho, J.-R. and Y.-J. Ahn (2022). "Investigation of mechanical behaviors of functionally graded CNT-reinforced composite plates." *Polymers 14*(13): 2664.

Dai, K., et al. (2003). "Comparison between the radial point interpolation and the Kriging interpolation used in meshfree methods." *Computational Mechanics 32*: 60-70.

Do, N.-T. and Q.-H. Pham (2023). "Dynamic analysis of bio-inspired helicoid laminated composite plates resting on Pasternak foundation excited by explosive loading." *Defence Technology 30*: 126-140.

Do, N.-T., et al. (2023). "Free vibration analysis of bio-inspired helicoid laminated composite plates resting on elastic foundation using isogeometric analysis and artificial neural network." *Mechanics of Time-Dependent Materials*: 1-24.

Fleming, M., et al. (1997). "Enriched element-free Galerkin methods for crack tip fields." *International journal for numerical methods in engineering 40*(8): 1483-1504.

Gao, Y., et al. (2022). "A new bending model for composite laminated shells based on the refined zigzag theory." *Archive of Applied Mechanics 92*(10): 2899-2915.

Greco, L., et al. (2023). "Design and analysis of energy absorbent bioinspired lattice structures." *Journal of Bionic Engineering 20*(4): 1670-1686.

Greenfeld, I. and H. D. Wagner (2023). "Crack deflection in laminates with graded stiffness—lessons from biology." *Bioinspiration & Biomimetics 18*(3): 036001.

Gu, L. (2003). "Moving kriging interpolation and element-free Galerkin method." *International journal for numerical methods in engineering 56*(1): 1-11.

Guellil, M., et al. (2021). "Influences of porosity distributions and boundary conditions on mechanical bending response of functionally graded plates resting on Pasternak foundation." *Steel and Composite Structures 38*(1): 1-15.

Hadji, M., et al. (2023). "Combined influence of porosity and elastic foundation parameters on the bending behavior of advanced sandwich structures." *Steel and Composite Structures 46*: 1-13.

Han, Q., et al. (2020). "Study on impact resistance behaviors of a novel composite laminate with basalt fiber for helical-sinusoidal bionic structure of dactyl club of mantis shrimp." *Composites Part B: Engineering 191*: 107976.

Hebali, H., et al. (2022). "Effect of the variable visco-Pasternak foundations on the bending and dynamic behaviors of FG plates using integral HSDT model." *Arch. Appl. Mech 83*(2): 177-191.

Jiang, H., et al. (2019). "Low-velocity impact resistance behaviors of bio-inspired helicoidal composite laminates with non-linear rotation angle based layups." *Composite Structures 214*: 463-475.

Katsikadelis, J. T. and A. Armenakas (1984). "Plates on elastic foundation by BIE method." *Journal of Engineering Mechanics 110*(7): 1086-1105.

Kerr, A. D. (1964). "Elastic and viscoelastic foundation models." *J. Appl. Mech 31*: 491-498.

Keshtegar, B., et al. (2020). "Wave propagation and vibration responses in porous smart nanocomposite sandwich beam resting on Kerr foundation considering structural damping." *Thin-Walled Structures 154*: 106820.

Khandan, R., et al. (2012). "The development of laminated composite plate theories: a review." *Journal of Materials Science 47*(16): 5901-5910.

Kiakojouri, F., V. De Biagi and L. Abbracciavento (2023). "Design for robustness: Bio-inspired perspectives in structural engineering." *Biomimetics 8*(1): 95.

Körbelin, J., et al. (2021). "Damage tolerance and notch sensitivity of bio-inspired thin-ply Bouligand structures." *Composites Part C: Open Access 5*: 100146.

Le, T. D. M. and V. N. Van Do (2024). Moving Kriging Meshfree Method and Kirchhoff Plate Theory for Free Vibration and Thermal Buckling Analysis of Advanced Material Plates. *Proceedings of the Third International Conference on Sustainable Civil Engineering and Architecture*, Singapore, Springer Nature Singapore.

Liu, J., et al. (2020). "The response of bio-inspired helicoidal laminates to small projectile impact." *International Journal of Impact Engineering 142*: 103608.

Liu, G., et al. (2022a). "Dynamics of imperfect inhomogeneous nanoplate with exponentially-varying properties resting on viscoelastic foundation." *European Journal of Mechanics-A/Solids 95*: 104649.

Liu, R., et al. (2022b). "Study on functional mechanical performance of honeycomb array structures inspired by gideon beetle." *Journal of Bionic Engineering 19*(4): 1024-1035.

Liu, R., et al. (2023). "Mechanical characteristics analysis of 3d-printing novel chiral honeycomb array structures based on functional principle and constitutive relationship." *Journal of Bionic Engineering 20*(5): 1917-1929.

Lu, T., et al. (2023). "Optimization design and nonlinear bending of bio-inspired helicoidal composite laminated plates." *Materials 16*(13): 4550.

Meo, M., et al. (2021). "Bioinspired helicoidal composite structure featuring functionally graded variable ply pitch." *Materials 14*(18): 5133.

Merazka, B., et al. (2021). "Hygro-thermo-mechanical bending response of FG plates resting on elastic foundations." *Steel and Composite Structures 39*: 631-643.

Mindlin, R. D. (1951). "Influence of Rotatory Inertia and Shear on Flexural Motions of Isotropic, Elastic Plates." *Journal of Applied Mechanics 18*(1): 31-38.

Mudhaffar, I. M., et al. (2021). "Hygro-thermo-mechanical bending behavior of advanced functionally graded ceramic metal plate resting on a viscoelastic foundation." *Structures 33*: 2177-2189.

Nguyen, N. T., et al. (2014). "Crack growth modeling in elastic solids by the extended meshfree Galerkin radial point interpolation method." *Engineering Analysis with Boundary Elements 44*: 87-97.

Nguyen, N. T., et al. (2020). "Meshfree thermomechanical crack growth simulations with new numerical integration scheme." *Engineering Fracture Mechanics 235*: 107121.

Nguyen, N. T., T. Q. Bui and T. T. Truong (2017). "Transient dynamic fracture analysis by an extended meshfree method with different crack-tip enrichments." *Meccanica 52*(10): 2363-2390.

Noor, A. K. (1975). "Stability of multilayered composite plates." *Fibre Science and Technology 8*(2): 81-89.

Odeh, A., et al. (2024). "Analysis of laminated composite plates: a comprehensive bibliometric review." *Buildings 14*(6): 1574.

Pant, M., I. V. Singh and B. Mishra (2010). "Numerical simulation of thermo-elastic fracture problems using element free Galerkin method." *International Journal of Mechanical Sciences 52*(12): 1745-1755.

Paruthi, S., et al. (2023). "Thermal-based free vibration and buckling behavior of bio-inspired cross-and double-helicoidal/bouligand laminated composite plates." *Acta Mechanica Solida Sinica 36*(6): 933-942.

Pasternak, N. (1954). New Method for Calculation of Foundation on the Elastic Basement. Gosstroiizdat, Moscow, Russian.

Qin, B., et al. (2019). "A unified formulation for free vibration of laminated plate through Jacobi-Ritz method." *Thin-Walled Structures 144*: 106354.

Reddy, J. and A. Khdeir (1989). "Buckling and vibration of laminated composite plates using various plate theories." *AIAA journal 27*(12): 1808-1817.

Reddy, J. N. (2003). Mechanics of laminated composite plates and shells: theory and analysis, CRC Press.

San Ha, N. and G. Lu (2020). "A review of recent research on bio-inspired structures and materials for energy absorption applications." *Composites Part B: Engineering 181*: 107496.

Sayyad, A. and Y. Ghugal (2014). "On the Buckling of Isotropic, Transversely Isotropic and Laminated Composite Rectangular Plates." *International Journal of Structural Stability and Dynamics 14*: 32.

Setoodeh, A. and G. Karami (2004). "Static, free vibration and buckling analysis of anisotropic thick laminated composite plates on distributed and point elastic supports using a 3-D layer-wise FEM." *Engineering Structures 26*(2): 211-220.

Shen, H.-S., J. J. Zheng and X. L. Huang (2003). "Dynamic response of shear deformable laminated plates under thermomechanical loading and resting on elastic foundatios." *Composite Structures - COMPOS STRUCT 60*: 57-66.

Sherman, J., W. Zhang and J. Xu (2021). "Energy absorption performance of bio-inspired honeycombs: numerical and theoretical analysis." *Acta Mechanica Solida Sinica 34*: 884-894.

Tahir, S. I., et al. (2022). "The effect of three-variable viscoelastic foundation on the wave propagation in functionally graded sandwich plates via a simple quasi-3D HSDT." *Steel and Composite Structures 42*(4): 501.

Thai, C. H., et al. (2016). "An improved moving Kriging meshfree method for plate analysis using a refined plate theory." *Computers & Structures 176*: 34-49.

Thai, C. H., et al. (2018). "A moving Kriging meshfree method with naturally stabilized nodal integration for analysis of functionally graded material sandwich plates." *Acta Mechanica 229*(7): 2997-3023.

Thai, H.-T. and D.-H. Choi (2013). "A simple first-order shear deformation theory for laminated composite plates." *Composite Structures 106*: 754-763.

Vu-Tan, V. and S. Phan-Van (2018). A modified moving kriging interpolation-based meshfree method with refined sinusoidal shear deformation theory for analysis of functionally graded plates. *Proceedings of the International Conference on Advances in Computational Mechanics 2017: ACOME 2017,* 2 to 4 August 2017, Phu Quoc Island, Vietnam, Springer.

Wang, H., et al. (2021). "Insights into the high-velocity impact behaviour of bio-inspired composite laminates with helicoidal lay-ups." *Polymer Testing 103*: 107348.

Wang, J. and G. Liu (2002). "A point interpolation meshless method based on radial basis functions." *International Journal for Numerical Methods in Engineering 54*(11): 1623-1648.

Wenting, Y., et al. (2021). "Nano-Tribological Properties of Bio-Inspired Laminated Graphene Reinforced Aluminum Martrix Composite." *Tribology 42*(2): 338-346.

Yokoyama, T. (1988). "Parametric instability of Timoshenko beams resting on an elastic foundation." *Computers & Structures 28*(2): 207-216.

Zaitoun, M. W., et al. (2023). "An efficient computational model for vibration behavior of a functionally graded sandwich plate in a hygrothermal environment with viscoelastic foundation effects." *Engineering with Computers 39*(2): 1127-1141.

Zhang, H., et al. (2018). "A simple first-order shear deformation theory for vibro-acoustic analysis of the laminated rectangular fluid-structure coupling system." *Composite Structures 201*: 647-663.

Zheng, Z., et al. (2021). "Experimental and theoretical studies of FRP-Steel composite plate under static tensile loading." *Construction and Building Materials 271*: 121501.

Zhou, Y., H. Cui and W. Wen (2022). "Mechanical behavior of 3D woven variable thickness composite plate under tensile loading." *Fibers and Polymers 23*(3): 819-826.